J Therm Anal Calorim (2014) 116:435–446
DOI 10.1007/s10973-013-3542-0

Thermal degradation mechanism of highly filled nano-SiO_2 and polybenzoxazine

Isala Dueramae · Chanchira Jubsilp · Tsutomu Takeichi · Sarawut Rimdusit

Received: 16 July 2013 / Accepted: 12 November 2013 / Published online: 8 December 2013

Abstract Effects of high nano-SiO_2 loading (up to 30 mass%) on polybenzoxazine (PBA-a) thermal degradation kinetics have been investigated using nonisothermal thermogravimetric analysis (TG). The DTG curves revealed three stages of thermal decomposition process in the neat PBA-a, while the first peak at low temperature was absent in its nanocomposites. As a consequence, the maximum degradation temperature of the nanocomposites shifted significantly to higher temperature as a function of the nano-SiO_2 contents. Moreover, the degradation rate for every degradation stage was found to decrease with the increasing amount of the nano-SiO_2. From the kinetics analysis, dependence of activation energy (E_a) of the nanocomposites on conversion (α) suggests a complex reaction with the participation of at least two different mechanisms. From Coats–Redfern and integral master plot methods, the average E_a and pre-exponential factor (A) of the nanocomposites showed systematically higher value than that of the PBA-a, likely from the shielding effect of the nanoparticles. The main degradation mechanism of the PBA-a was determined to be a random nucleation type with one nucleus on the individual particle (F1 model), while that of the PBA-a nanocomposite was the best described by diffusion-controlled reaction (D3 model).

Keywords Polybenzoxazine · Nano-SiO_2 · Nanocomposites · Thermal degradation · Kinetics

I. Dueramae · S. Rimdusit (✉)
Polymer Engineering Laboratory, Department of Chemical Engineering, Faculty of Engineering, Chulalongkorn University, Bangkok 10330, Thailand
e-mail: sarawut.r@chula.ac.th

C. Jubsilp
Department of Chemical Engineering, Faculty of Engineering, Srinakharinwirot University, Ongkharak, Bangkok, Nakhon Nayok 26120, Thailand

T. Takeichi
Department of Environmental and Life Sciences, Toyohashi University of Technology, 1-55 Hibarigaoka, Tempaku-cho, Toyohashi 441-8580, Japan

Introduction

Polybenzoxazines (PBZs) are a relatively novel class of thermosetting phenolic resin that is attracting much attention as they possess various advantageous characteristics that overcome the limitations of conventional phenolic and epoxy resins, such as high thermal stability, high glass transition temperature, high modulus, low water absorption, low dielectric constant, and near-zero shrinkage upon curing [1, 2]. In addition, the curing of benzoxazine resin can occur without any acid catalysts or producing any by-products that minimizing void formation in the final product. Moreover, the monomer shows very low melt viscosity providing its ease of compounding with various fillers or extenders [1–3]. In recent years, PBZs have gained much attention in both industrial and academic areas [1–5]. Henkel AG & Co. KGaA recently launches Henkel Benzoxazine Resin 99110TM for a wide range of aircraft applications [4], whereas Huntsman [5] advanced materials has already commercialized five types of solid benzoxazine resins as a new generation of halogen-free materials for a broad range of advanced applications.

One critical research field on PBZs is to utilize and to better understand their relatively high thermal stability. In the recent reports, a thermal degradation behaviors of PBZs has been investigated by TG, TG-interfaced with a Fourier transform infrared spectrometer (TG-FTIR), or evolved gas

analysis performed by GC–MS, and DP-MS [6–9]. In the case of neat PBZs, the side functional groups abbreviated as "R" of a Mannich base, $–CH_2–NR–CH_2–$, were found to be the weakest point in the cross-linked network structures when heat is applied [7]. Therefore, ''end-capping'' of these functionality has been proposed to stabilize the Mannich base, with the expectation of further improvement of the thermal stability of the PBZs. The main methods are to introduce reactive functional groups or another heat-resistant component into the benzoxazine systems [10]. These methods are complex and difficult to actualize because new resin systems need to be prepared and thoroughly examined for the resulting properties. An addition of suitable and inert inorganic filler into the polymers is reported to be one highly effective approach to improve their thermal stability as well as flammability [11, 12]. One crucial way to improve flame retardation in polymers is by promoting the formation of stable char since the char layer can act as a thermal insulator and a barrier to oxygen diffusion [11, 12]. An addition of the inherently stable inorganic phase was reported to augment the char formation by making the char more voluminous and mechanically stronger, consequently improving its insulating and barrier properties [11].

The effects of different nanoparticles on various types of polymer thermal stability have been investigated [11–24]. Chrissafis et al. [15] considered the effects of different nanofillers e.g., MMT, MWCNTs, and hydrophobic $cSiO_2$ nanoparticles (dimethylchlorosilane-treated nanosilica) at a fixed content of 2.5 mass% on thermal degradation of HDPE. The authors reported that thermal stability of HDPE was enhanced by the incorporation of different nanoparticles. The degradation kinetics of HDPE and its nanocomposites were found to be the same and the best described by two consecutive mechanisms of nth order autocatalysis. However, the authors reported that the activation energy of the nanocomposites was higher than that of HDPE i.e., 140 kJ mol^{-1} for HDPE versus 230 kJ mol^{-1} for HDPE/$cSiO_2$ of the first reaction mechanism and 260 kJ mol^{-1} for HDPE versus 290 kJ mol^{-1} for HDPE/$cSiO_2$ of the second reaction mechanism [13].

In various studies, published recently, an addition of nanoparticles was reported to substantially increase thermal stability of many polymers [11–25]. Laachachi et al. [21] reported an improvement in the degradation temperature at 2 % mass loss of PMMA of 17 °C when 15 mass% of Al_2O_3 nanoparticles was incorporated in the polymer. Similar characteristics were also observed in the thermal degradation of epoxy [12]. The presence of nanoscale silica in epoxy matrix from 0 to 30 mass% was found to level up the thermal stability (T_d) as well as the activation energy values of the degradation reaction of the epoxy.

In the highly filled nanocomposite system, some research studies have evaluated the effects of nanoparticles on the polymer matrix thermal stability [12, 21]. However, few articles were dealing with the effect of high filler loading on thermal decomposition mechanism. From the aforementioned reports, the factors influencing thermal stability of the filled polymers not only depend on the individual thermal stability of the matrix polymer and the nanoparticles, but also on the amount of filler used, dispersion uniformity, as well as the degree of interaction between the inorganic filler and the matrix. Therefore, ideal thermally stable performance is achieved using nanoparticles that are able to uniformly disperse thoroughly in the matrix and interact strongly with the organic matrix. In our recent study, an ability of bisphenol-A based benzoxazine resin (BA-a) to be highly filled with nano-SiO_2 particles up to 30 mass% with negligible void was achieved [22]. The PBA-a/nano-SiO_2 composites showed significantly higher thermomechanical properties than those of the recently reported nano-SiO_2 filled epoxy [23] or cyanate ester [24]. This property enhancement is likely due to the strong interfacial bonding through –Si–O–C linkages between the nano-SiO_2 and the PBA-a [22].

The knowledge of the kinetic model driving a process provides a valuable insight regarding the reaction mechanism and it is useful for controlling a process, determining optimum processing temperature or for aging [26]. Consequently, the understanding of the thermal stability and thermal decomposition kinetics of materials makes it possible to develop and extend their applications as various industrial fields.

It is believed that the ability of the nano-SiO_2 to form Si–O–C bonds with PBA-a can significantly alter thermal degradation mechanisms and decomposition behaviors of the PBA-a in a positive manner [3, 22]. The aim of the present study, therefore, is to evaluate the effect of high nano-SiO_2 loading on thermal decomposition kinetic parameters of the PBA-a, e.g., activation energy (E_a), pre-exponential factor (A), and the conversion function $f(\alpha)$ by using three well-known methods, i.e., Kissinger method, Flynn–Wall–Ozawa method, Coats–Redfern method, and master plots based on the integral form of the kinetic data method. The strong interfacial bonding above should also be more clearly observed in the highly filled system of the nano-SiO_2 in the PBA-a.

Materials and methods

Materials

Benzoxazine monomer, bis(3-phenyl-3,4-dihydro-2H-1,3-benoxzinyl)isopropane (BA-a), was synthesized from 2,2′-bis(4-hydroxyphenyl)-propane (bisphenol-A) with aniline and formaldehyde according to the solventless method

described elsewhere [27]. Bisphenol-A (polycarbonate grade) provided by Thai Polycarbonate Co., Ltd. was used as received. Para-formaldehyde (AR grade) and aniline (AR grade) were purchased from Merck Ltd.

Nano-SiO_2 (Reolosil® QS-20) is a product of Tokuyama Co., Tokyo, Japan. The nano-SiO_2 has a density of 2.203 g cm^{-3}. An average diameter of primary particles of the filler is ranging from 5 to 50 nm with average specific surface area of about 200 m^2 g^{-1}. It has fluffy and white powder characteristics of amorphous structure.

Sample preparations

The benzoxazine (BA-a) resin was well dry-mixed with nano-SiO_2 at a desired mass fraction. The BA-a/nano-SiO_2 mixture was then heated up to 100 °C and mechanically mixed to ensure nano-SiO_2 particles wet-out by the BA-a resin. The nano-SiO_2/BA-a compound in the form of paste was then compression-molded. All the specimens were thermally cured at 200 °C under a pressure of 0.1 MPa for 3 h. The fully cured specimens were left to cool down at room temperature before their characterizations.

Thermogravimetric analysis

Thermogravimetric analysis (TG) of nano-SiO_2-filled PBZ composites was performed using Rigaku Thermo Plus 2 TG–DTA TG8120. Samples (10–15 mg) were heated from 50 to 850 °C at constant heating rates of 5, 10, 15 and 20 °C min^{-1} under argon atmosphere with a flow rate of 80 mL min^{-1}.

Results and discussion

TG of nano-SiO_2 filled polybenzoxazine

Figure 1 shows the thermogravimetric data and the corresponding derivative thermogravimetry (DTG) curves of neat PBA-a resin and PBA-a/nano-SiO_2 composites under argon atmosphere at 10 °C min^{-1} of heating rates. As the TG plot, the degradation temperature at 5 % mass loss and solid residue of the nanocomposites at 800 °C systematically increased with the increasing the nano-SiO_2 content as shown in Table 1. To clarify the effect of the different percentages of filler on the thermal stability, the integral procedure decomposition temperature (IPDT) was determined. The IPDT proposed by Doyle [28] correlates the volatile parts of polymeric materials and was used for estimating their inherent thermal stability [28, 29]. IPDT was calculated from Eq. 1.

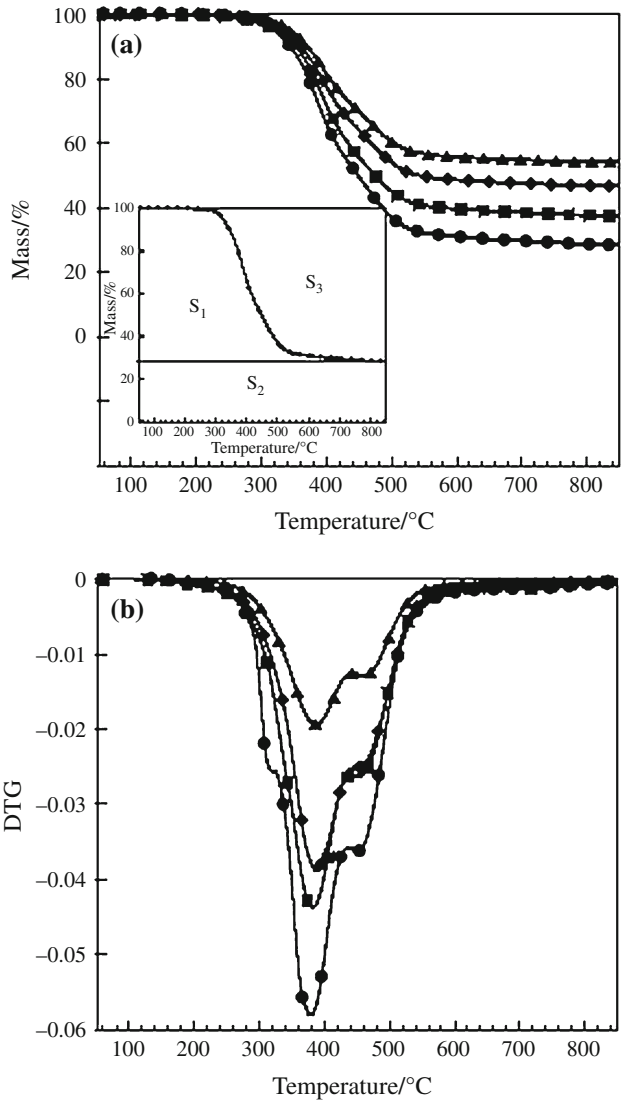

Fig. 1 **a** Thermogravimetric and **b** DTG curves of (*filled circle*) PBA-a, and their composites at various nano-SiO_2 contents: *filled square* 10 mass%, *filled diamond* 20 mass%, *filled triangle* 30 mass%. *Inset* schematic representation of S_1, S_2 and S_3 for A^* and K^*

Table 1 Thermal stability parameters calculated from the TG curves

Nano-SiO_2 content/ mass%	T_d at 5 % mass loss/°C	Solid residue at 800 °C/%	A^*	K^*	IPDT/°C
0	315	29	0.6037	1.8984	967
10	322	38	0.6471	2.3782	1,281
20	332	46	0.7341	2.1334	1,303
30	338	55	0.7463	2.5187	1,554

$$\text{IPDT } (^{\circ}\text{C}) = A^*K^*(T_f - T_i) + T_i, \quad (1)$$

$$A^* = (S_1 + S_2)/(S_1 + S_2 + S_3), \quad (2)$$

$$K^* = (S_1 + S_2)/S_1, \quad (3)$$

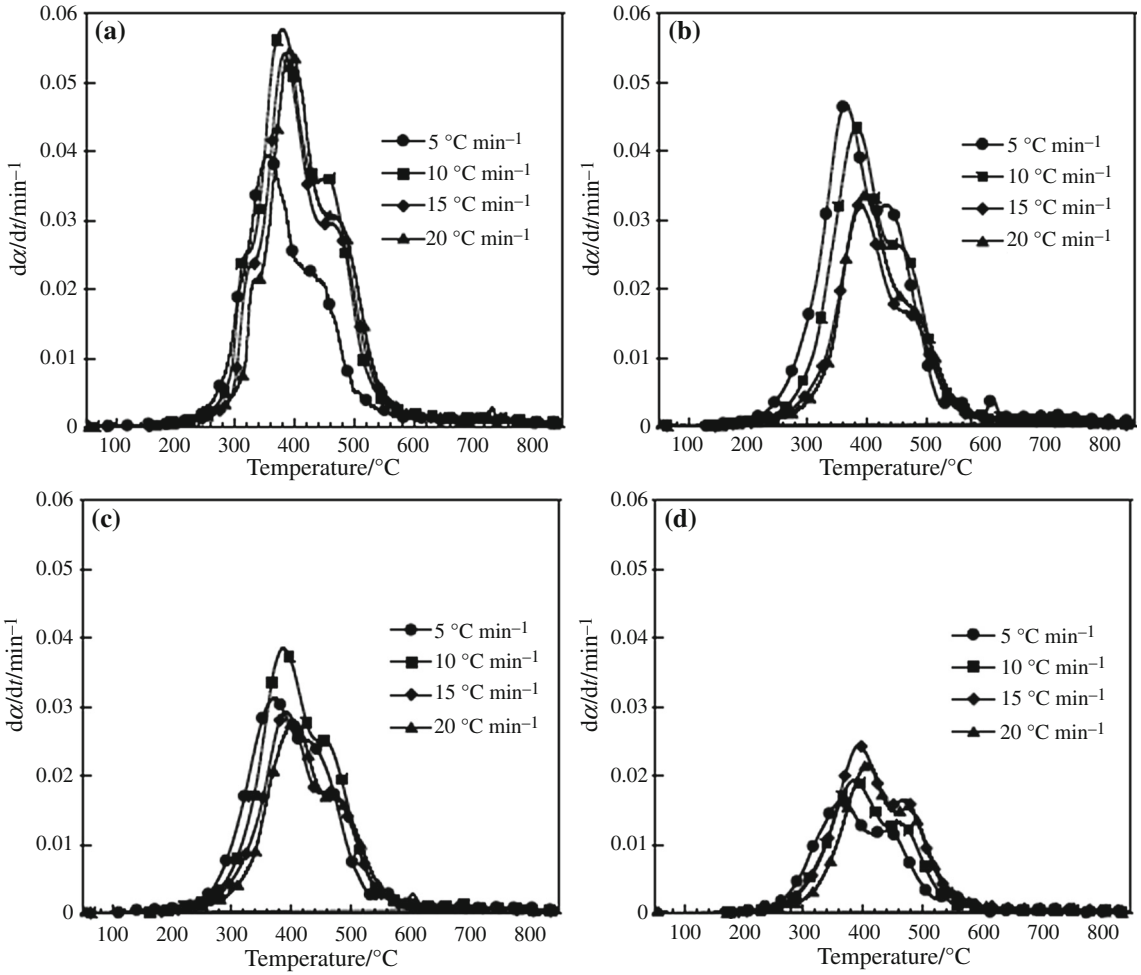

Fig. 2 DTG curve (**a**) PBA-a, and their composites at various nano-SiO_2 contents: **b** 10 mass%, **c** 20 mass%, **d** 30 mass%

where A^* is the area ratio of a total experimental curve defined by total TG curve. K^* is the coefficient of A^* while T_i is the initial experimental temperature (50 °C in this study). T_f is the final experimental temperature i.e., 850 °C. S_1, S_2, and S_3 are the areas of the three regions in TG plot shown in an inset of Fig. 1a. The results of IPDT parameters (A^* and K^*) of thermal stability are listed in Table 1. As a result, IPDT greatly increases from 967 °C for the neat PBA-a to 1,554 °C for the nanocomposites containing 30 mass% by mass of nano-SiO_2. This suggests that the nano-SiO_2 can improve the thermal stability of the neat PBA-a. Furthermore, the high melting point of nano-SiO_2 can serve as a good thermal cover layer, avoiding the direct thermal decomposition of polymer matrix by heat. It is well known that when inorganic filler particles are dispersed in the polymeric matrix, the formed layers are impermeable toward small molecular gases or volatile products that are generated during decomposition and a much longer path around the nanoparticles is needed for their removal from the decomposed matrix [30]. The effects should be more pronounced when nanoparticles with tremendous surface area such as nano-SiO_2 is used as a dispersed phase. Surprisingly, the thermal degradation behavior of the nanocomposites clearly differ from neat PBA-a as evidenced in Fig. 1b. Three overlapped curves in neat PBA-a become two overlapped curves for nanocomposites. We hypothesized that the thermal degradation mechanism of the nanocomposties can be altering from neat resin. The kinetic model driving a process provides a valuable insight regarding the thermal degradation mechanism. DTG is a powerful tool for characterizing the kinetic parameters of thermal reactions applying various analytical techniques, due to its uniqueness with respect to the kinetic parameters. This uniqueness may also derive from the peak temperature because of their proven relationships with activation energy [31].

For further kinetic studies of the nanocomposite systems, DTG curves (first derivative of TG curve) of PBA-a and its nanocomposites at different heating rate are plotted as shown in Fig. 2a–d. This figure clearly shows that

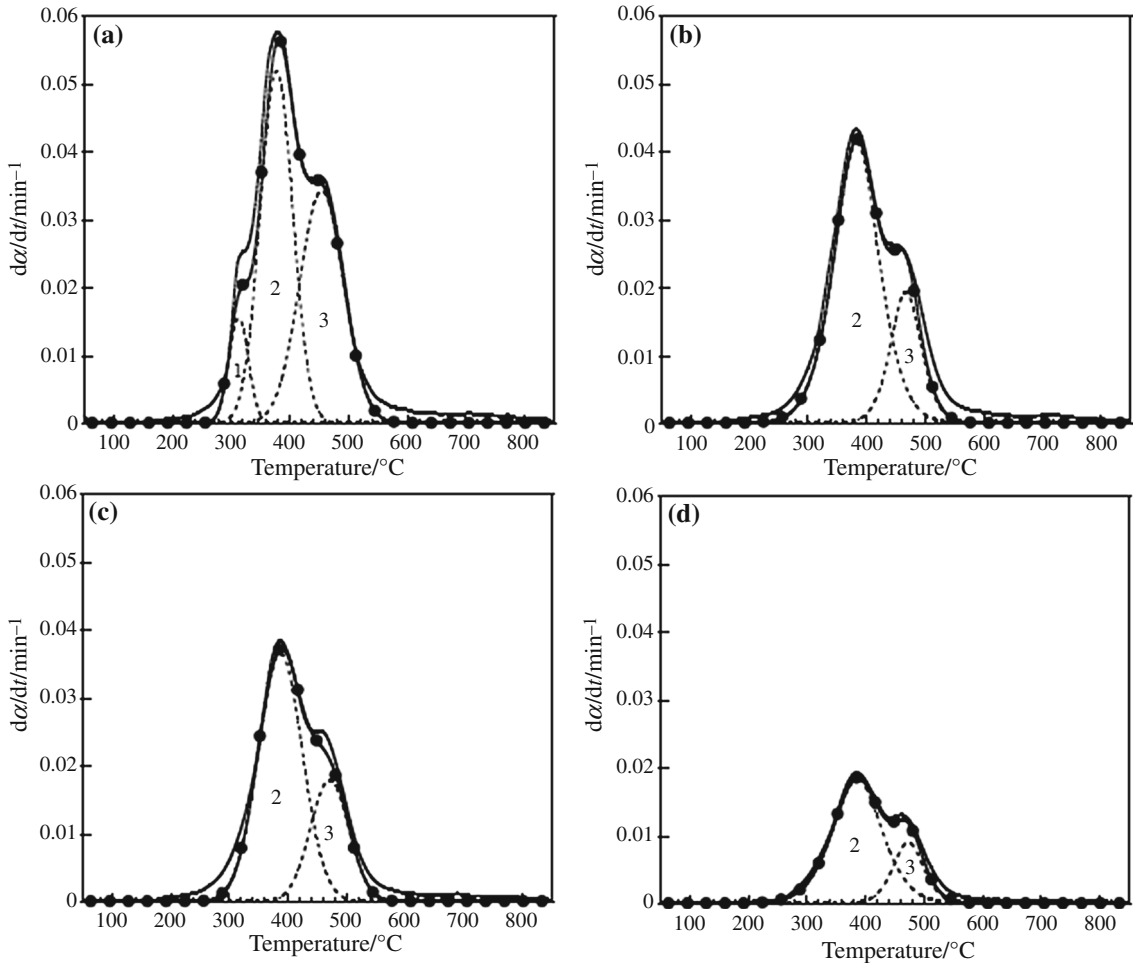

Fig. 3 DTG curve and individual contributions of (**a**) PBA-a, $R^2 = 0.9962$; and their composites at various nano-SiO_2 contents: **b** 10 mass%, $R^2 = 0.9982$; **c** 20 mass%, $R^2 = 0.9993$; **d** 30 mass%, $R^2 = 0.9978$. *Solid line* experimental data, *filled circle* simulated curve at 10 °C min^{-1}, *dotted line* deconvolution of each stages

increasing the heating rate enables the DTG curve to shift toward a higher temperature range, which means that increased mass loss rate of the thermal degradation reactions will occur at a higher temperature.

All DTG curves of the matrix and it nanocomposites were separated using Peakfit® program as exemplified in Fig. 3a–d After resolving the curves by the computer software, it can be noticed that the DTG curve of the PBA-a, presented in Fig. 3a, composes of a three-stage mass-loss process. This result is in good agreement with the previous studies [7]. This degradation process was observed by FTIR with the middle peak having the highest maximum rate of mass loss which is phenol-substituted compounds and the evolved gas of the final stage are similar with the main stage, while the various amines were detected in first stage [7]. The volatile products emitted during the thermal decomposition processes of aromatic amine-based PSZs were identified in more details by using GC–MS [8] and DP-MS techniques [9]. The decomposition products were divided into eight categories as follows: benzene derivatives, amines, phenolic compounds, 2,3-benzofuran derivatives, isoquinoline derivatives, biphenyl compounds, Mannich base compounds, and phenanthridine derivatives [8]. In addition, the overlapped curve in PBA-a indicated that the degradation of the phenolic linkage occurs simultaneously with the degradation of the Mannich base, but the onset of each type of degradation is different [7].

The difference in thermal degradation pattern was observed in the PBA-a nanocomposites i.e., the disappearance of thermal degradation at first stage. The decomposition processes were reduced to two major events in the nanocomposites as clearly seen. Moreover, the maximum decomposition rates were decreased significantly from 0.058 to 0.045, 0.039, and 0.02 % $°C^{-1}$, whereas the peak positions of the maximum decomposition rates were shifted to higher temperature i.e., 362, 373, 385, 400 °C with the increasing nano-SiO_2 contents from 0, 10, 20, and 30 mass%, respectively, as shown in Fig. 3a–d.

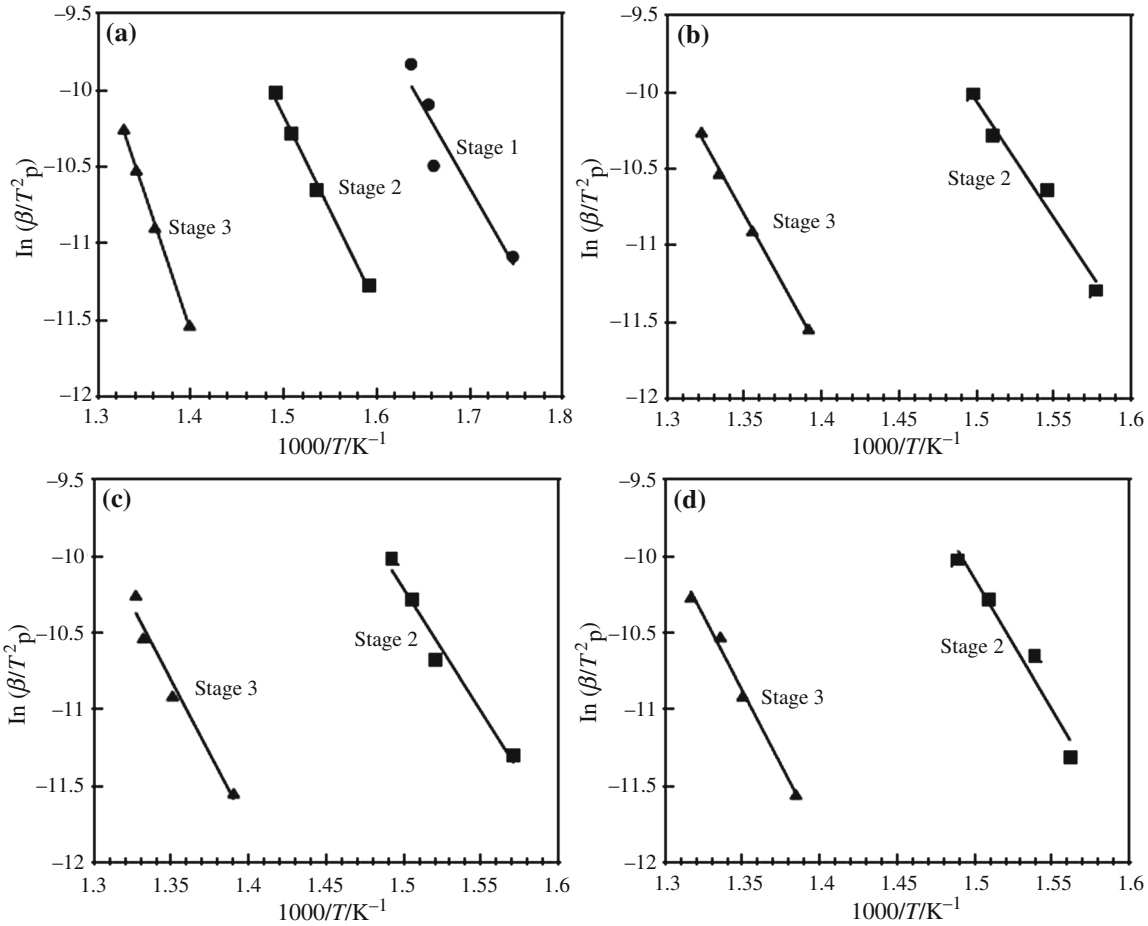

Fig. 4 Plots of ln β/T_p^2 versus $1000/T_p$ at different heating rates according to Kissinger method for the **a** PBA-a, and their composites at various nano-SiO_2 contents: **b** 10 mass%, **c** 20 mass%, and **d** 30 mass%

Thermal degradation kinetics parameters of nano-SiO_2 filled PBA-a system

In order to analyze more thoroughly the effects of the nanoparticles on the degradation mechanism of PBA-a, it is important to determine the kinetic parameters of the thermally degraded composite products. After all the overlapped DTG peaks were resolved, the conversions were calculated from the areas under each peak. Then, the E_a of each decomposition stage was obtained via kinetic analysis.

For nonisothermal TG [32, 33], Kissinger method uses Eq. 4 to determine the E_a of solid state reactions [34].

$$\ln\left(\frac{\beta}{T^2}\right) = \ln\frac{AR}{E_a} + \ln\left[n(1-\alpha_p)^{n-1}\right] - \frac{E_a}{RT_p}, \quad (4)$$

where T_p and α_p are the absolute temperature and mass loss at maximum mass loss rate $(\alpha_p/dt)_p$, respectively, and n is the reaction order. A is the pre-exponential factor (min^{-1}) and R is the gas constant (8.314 J mol^{-1} K^{-1}). The advantage of the Kissinger model is that the E_a can be obtained without the knowledge of any thermal degradation reaction mechanism in advance and also widely used in the analysis of structural transformations because of its simplicity and accuracy [32, 33]. For a series of experiments performed at different heating rates (β), the E_a can be calculated from the slope of the plot of $\ln(\beta/T_p^2)$ versus $1{,}000/T_p$ as presented in Fig. 4a–d for PBA-a and it

Table 2 Activation energies obtained by using Kissinger method and Flynn–Wall–Ozawa method for polybenzoxazine and theirs nanocomposites

Nano-SiO_2 content/mass%	E_a/kJ mol^{-1}					
	Kissinger method			Flynn–Wall–Ozawa method		
	Stage 1	Stage 2	Stage 3	Stage 1	Stage 2	Stage 3
0	96	111	126	72	119	149
10		133	155		148	169
20		145	180		140	167
30		153	190		140	218

nanocomposites. The numerical results are also summarized in Table 2. From the table, it is clearly seen that the activation energy showed a substantially greater value when the nanoparticles were added in the PBA-a. The trend was also consistency with the enhancement of the T_d and IPDT with the amount of the nanofiller.

Kissinger method provides the best accuracy for a single-step process. In the case of complex mechanisms or for transformations involving more than one step, an adequate representation of the commonly encountered multistep kinetics would normally require more than a single value of the activation energy [33]. Therefore, it is necessary to use an isoconversional method to back up the validity of the Kissinger estimates.

Isoconversional analysis of nano-SiO_2 filled PBA-a system

Flynn–Wall–Ozawa method (model-free) is an integral isoconversional method [33, 35], which assumes that the conversion function $f(\alpha)$ does not change with the variation of the heating rate for all values of degree of conversion α. It involves measuring the temperatures corresponding to given values of conversion (α) from experiments at different heating rates (β). Therefore, plotting log (β) against $1/T$ in form of Eq. 5:

$$\ln\beta = \ln\frac{AE_a}{g(\alpha)} - 2.315 - \frac{0.457E_a}{RT}, \quad (5)$$

where $g(\alpha)$ is the integrated form of the kinetic rate as shown in Table 3. The values of E_a were calculated from the slope of the straight lines log β versus $1/T$. The E_a for different conversion values of 0, 10, 20, and 30 mass% nano-SiO_2 filled PBA-a nanocomposites are shown in Fig. 5a–d, respectively. At 0, 10, and 20 mass% nano-SiO_2 contents and for all stages of the thermal degradation, the dependence of E_a on α value exhibited a linear increasing tendency as seen in Fig. 5a–c. An increase of E_a with increasing is a relatively common phenomenon and is frequently observed in many polymers [14]. On the other hand, the 30 mass% nano-SiO_2 filled PBA-a exhibited a relatively constant E_a with conversion particularly over the 20–80 % conversion range. Montero et al. [25] reported that E_a of 2.5 mass% POSS contained epoxy is approximately constant in the conversion range of 0.3–0.8. Furthermore, our nanocomposite systems showed substantially higher values of E_a than the neat PBA-a as seen in Table 2. The phenomenon is attributed to the difficulty to liberate decomposition gases from the matrix containing inorganic particles like nano-SiO_2.

In general, a variation of E_a with conversion in our specimens indicated that the reaction mechanism of their thermal decomposition is a relatively complex reaction mechanism that invalidates the separation of variables involved in the Flynn–Wall–Ozawa analysis [35]. As polymer degradation processes usually involve chain reactions, *f()* in reaction rate equation [32, 33] will represent a series of elemental steps being a function of conversion with each step having its own kinetic parameters.

The kinetic mechanisms can be accomplished using a simplified version of the Coats–Redfern method [36] in form of Eq. 6.

Table 3 Algebraic expressions of $f(\alpha)$ and $g(\alpha)$ for the reaction models [33]

Symbol	Reaction model	$f(\alpha)$	$g(\alpha)$
P3	Power law	$3\alpha^{2/3}$	$\alpha^{1/3}$
P4	Power law	$4\alpha^{3/4}$	$\alpha^{1/4}$
F1	Random nucleation with one nucleus on the individual particle	$1-\alpha$	$-\ln(1-\alpha)$
F2	Random nucleation with two nucleus on the individual particle	$(1-\alpha)^2$	$(1-\alpha)^{-1}-1$
F3	Random nucleation with three nucleus on the individual particle	$(1-\alpha)^3$	$1/2\left((1-\alpha)^{-2}-1\right)$
A2	Nucleation and growth (Avrami equation ($n=2$))	$2(1-\alpha)[-\ln(1-\alpha)]^{1/2}$	$[-\ln(1-\alpha)]^{1/2}$
A3	Nucleation and growth (Avrami equation ($n=3$))	$3(1-\alpha)[-\ln(1-\alpha)]^{2/3}$	$[-\ln(1-\alpha)]^{1/3}$
A4	Nucleation and growth (Avrami equation ($n=4$))	$4(1-\alpha)[-\ln(1-\alpha)]^{3/4}$	$[-\ln(1-\alpha)]^{1/4}$
D2	Two-dimensional diffusion (Valensi equation)	$[-\ln(1-\alpha)]^{-1}$	$(1-\alpha)\ln(1-\alpha)+\alpha$
D3	Three-dimensional diffusion (Jander equation)	$(3/2)\left[1-(1-\alpha)^{1/3}\right]^{-1}(1-\alpha)^{2/3}$	$\left[1-(1-\alpha)^{1/3}\right]^2$
R2	Phase boundary controlled reaction (contracting area)	$2(1-\alpha)^{1/2}$	$\left[1-(1-\alpha)^{1/2}\right]$
R3	Phase boundary controlled reaction (contracting volume)	$3(1-\alpha)^{2/3}$	$\left[1-(1-\alpha)^{1/3}\right]$

Average value from experimental result by heating rate of 5, 10, 15 and 20 °C min^{-1}

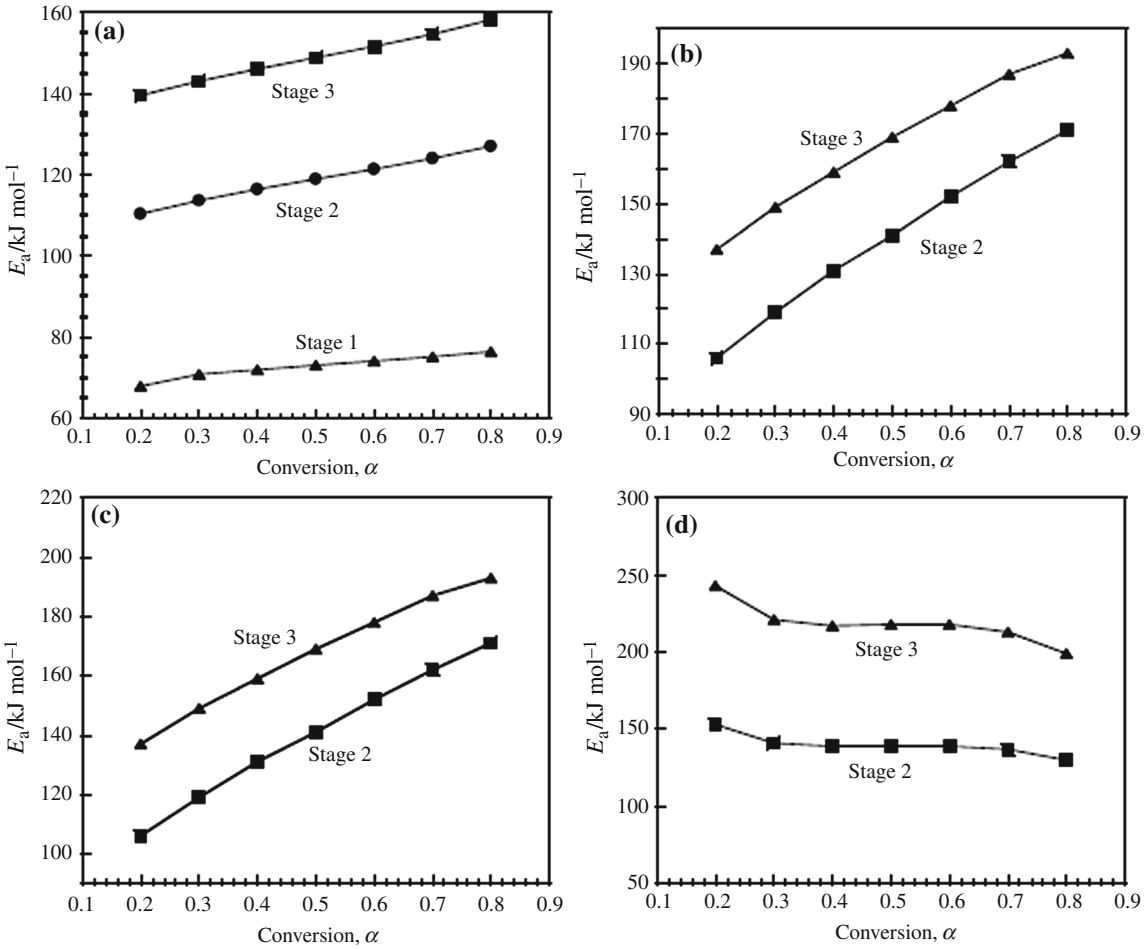

Fig. 5 Dependence of activation energy (E_a) on degree of the conversion (α) of the mass loss for second state process, as calculated with Flynn–Wall–Ozawa's method: **a** PBA-a, and their composites at various nano-SiO_2 contents: **b** 10 mass%, **c** 20 mass% and **d** 30 mass%

$$\ln\frac{g(\alpha)}{T^2} = \ln\left(\frac{AR}{\beta E_a}\right) - \frac{E_a}{RT}. \tag{6}$$

Accordingly, at a specific heating rate, the activation energy can be estimated for every $g(\alpha)$ of Eq. 6, as listed in Table 3, by plotting ($\ln [g(\alpha)/T^2]$) versus $1/T$. Table 4 lists the calculated kinetic parameters for different models at a heating rate of 10 °C min^{-1} of the maximum degradation stage. The value of the E_a and mechanism model were selected based on the E_a that was similar to the value obtained by isoconversional methods and showed linear trend with maximum correlation coefficient >0.98. Table 5 lists mechanism models that are sufficiently similar in shape and provide calculated values of the E_a close to the value obtained by the isoconversional methods. Coats–Redfern analysis was used to only explore the stages of the kinetic analysis. The selected models of our PBZ and its nanocomposites were then confirmed with the master plots based on the integral form of the kinetics.

Determination of the kinetic model by means of generalized master plots of nano-SiO_2 filled polybenzoxazine system

The kinetic rate equation at infinite temperature is obtained by introducing the generalized time, θ, which is defined in reference [37]. From the integral kinetic equation at infinite temperature in integral form, we can obtain the following equation using a reference point at $\alpha = 0.5$ as presented in Eq. 7.

$$\frac{g(\alpha)}{g(0.5)} = \frac{\theta(\alpha)}{\theta(0.5)} = \frac{p(x)}{p(0.5)}, \tag{7}$$

where $p(x)$ is in form of Eq. 8:

$$p(x) = \frac{e^{-x}}{x}\frac{x^3 + 18x^2 + 86x + 96}{x^4 + 20x^3 + 120x^2 + 240x + 120} \tag{8}$$

The $p(x)$ form was proposed by Perez-Maqueda and Criado [38], where x is E_a/RT and $\theta_{0.5}$ is the generalized time

Table 4 Values of E_a and A based on Coats–Redfern method for maximum stage process at heating rate of 10 °C min^{-1} for PBA-a and their nanocomposites

Type	E_a/kJ mol^{-1}	ln$A$/min^{-1}	R^2	Type	E_a/kJ mol^{-1}	ln$A$/min^{-1}	R^2
PBA-a				10 mass% nano-SiO_2-filled PBA-a			
P2	32	−3.75	0.9219	P2	14	−7.76	0.8785
P3	18	−6.85	0.8892	P3	8	−9.42	0.7974
P4	11	−8.62	0.8341	P4	8	−9.42	0.7974
F1	112	12.12	0.9917	F1	95	8.96	0.9927
F2	76	6.41	0.9056	F2	63	3.98	0.8990
F3	162	24.02	0.9162	F3	137	19.35	0.9121
A2	50	0.24	0.9894	A2	42	−1.43	0.9902
A3	30	−3.98	0.9863	A3	24	−5.17	0.9865
A4	20	−6.24	0.9818	A4	16	−7.21	0.9807
D2	182	23.84	0.9669	D2	156	19.06	0.9696
D3	207	27.40	0.9827	D3	159	17.83	0.9844
R2	92	7.36	0.9729	R2	78	4.72	0.9748
R3	98	8.23	0.9805	R3	83	5.43	0.9821
Type	E_a/kJ mol^{-1}	ln$A$/min^{-1}	R^2	Type	E_a/kJ mol^{-1}	ln$A$/min^{-1}	R^2
20 mass% nano-SiO_2-filled PBA-a				30 mass% nano-SiO_2-filled PBA-a			
P2	10	−8.70	0.8518	P2	10	−8.95	0.8582
P3	5	−10.32	0.7086	P3	5	−10.57	0.6829
P4	5	−10.32	0.7086	P4	5	−10.57	0.6829
F1	78	5.97	0.9935	F1	76	5.22	0.9919
F2	51	1.82	0.8896	F2	50	1.25	0.8878
F3	113	15.21	0.9062	F3	110	14.16	0.9053
A2	38	−2.52	0.9899	A2	33	−3.45	0.9883
A3	19	−6.33	0.9859	A3	18	−6.64	0.9823
A4	12	13.46	0.9774	A4	11	−8.45	0.9713
D2	129	14.45	0.9713	D2	127	13.33	0.9720
D3	157	17.9	0.9858	D3	154	18.47	0.9852
R2	64	2.18	0.9758	R2	62	1.55	0.9756
R3	68	2.75	0.9831	R3	67	2.08	0.9823

Table 5 Degradation mechanism based on Coat-Redfern method of all degradation stages

Type of samples	Stage 1	Stage 2	Stage 3
PBA-a	F1, F2, R2, R3	F1, R2, R3	F1, F3, D2, D3
10 mass% nano-SiO_2-filled PBA-a		F1, F3, D2, D3, R2, R3	F1, F2, F3, D2, D3
20 mass% nano-SiO_2-filled PBA-a		F3, D2, D3	F2, F3, D2, D3
30 mass% nano-SiO_2-filled PBA-a		F3, D2, D3	D2, D3

at $\alpha = 0.5$. The integral master plot method at infinite temperature can be constructed by comparing the experimental master plot of the reduced generalized time, $\theta/\theta_{0.5}$, against α with various theoretical master plots of $g(\alpha)/g(0.5)$ against α [38].

When $g(\alpha)/g(0.5)$ master curves can be plotted using Eq. 7, according to different reaction mechanism shown in Table 3. The experimental master curves were obtained using the determined value of the average E_a from isoconversional method. Comparison of the experimental plots of $\theta/\theta_{0.5}$ against α with the theoretical plots of $g(\alpha)/g(0.5)$ against α was made as shown in Figs. 6, 7, 8, and 9 for 0–30 mass% nano-SiO_2 filled PBA-a nanocomposites for all degradation range of each stage ($\alpha = 0$–1). It is clearly seen from insets of Figs. 6, 7, 8, and 9 that the overlapped thermal degradation range at the end of each stage is eliminated ($\alpha = 0$–0.7). The experimental master curves are agreed with the theoretical master curve corresponding to the F1, D3, D3 and D3 mechanisms for the

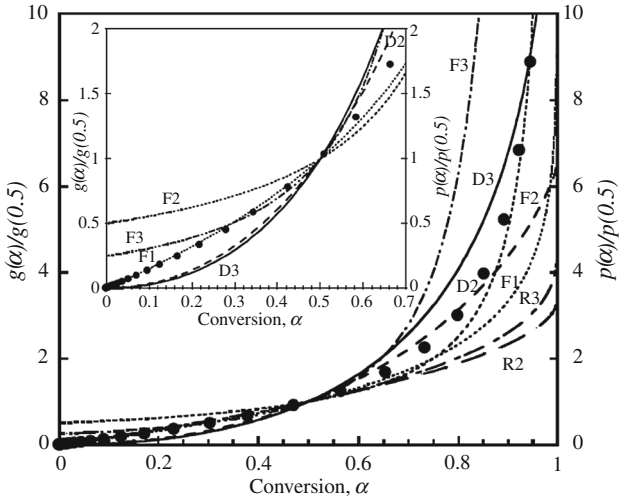

Fig. 6 Integral mater plot as a function of α at different mechanisms models of second degradation stage of PBA-a: *solid line* theoretical model and *filled circle* experimental data. *Solid line* theoretical model and *filled circle* experimental data. *Inset* integral mater plot as a function of α = 0–0.7

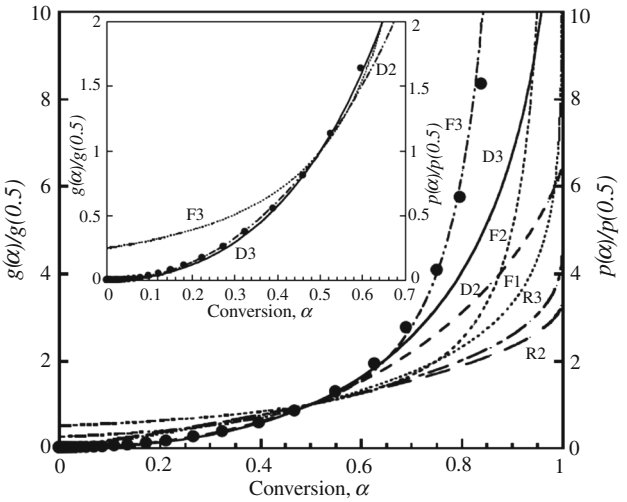

Fig. 8 Integral mater plot as a function of at different mechanisms models of second degradation stage of 20 mass% nano-SiO_2-filled PBA-a nanocomposites: *solid line* theoretical model and *filled circle* experimental data. *Inset* integral mater plot as a function of α = 0–0.7

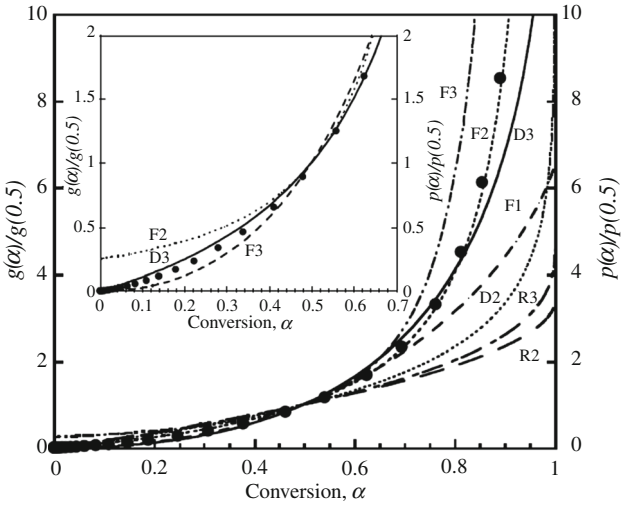

Fig. 7 Integral mater plot as a function of α at different mechanisms models of second degradation stage of 10 mass% nano-SiO_2-filled PBA-a nanocomposites

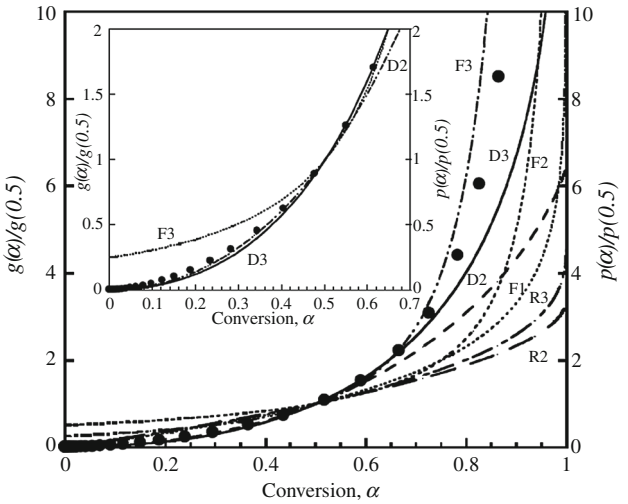

Fig. 9 Integral mater plot as a function of α at different mechanisms models of second degradation stage of 30 mass% nano-SiO_2-filled PBA-a nanocomposites: *solid line* theoretical model and *filled circle* experimental data. *Inset* integral mater plot as a function of α= 0–0.7

main degradation stage of 0, 10, 20, and 30 mass% of nano-SiO_2 filled PBA-a nanocomposites, respectively. The corresponding E_a and ln$A$ values for the most probable theoretical kinetic models were determined from Coats–Redfern method and the average values from the heating rates of 5, 10, 15, and 20 °C min^{-1} were obtained and listed in Table 6.

From the kinetic parameters for all degradation stages in Table 6, it is clearly seen that the average E_a and ln$A$ of each degradation stage increases with the addition of the nano-SiO_2. For example, the average E_a and ln$A$ in the main degradation stage are 116 kJ mol^{-1} and 13.6 for the neat PBA-a while the 10 mass% nano-SiO_2 filled PBA-a nanocomposite possesses an average E_a and ln$A$ of 157 kJ mol^{-1} and 19.1. Moreover, the relatively high nano-SiO_2 content (10–30 mass%) in our nanocomposites was found to provide similar values of the E_a and ln$A$ of the thermal degradation reaction.

Chissafis et al. [15] reported the calculated activation energy values of high density polyethylene (HDPE) and silica (5 mass%) to be higher than that of neat HDPE suggesting the evidence that SiO_2 causes stabilization in thermal decomposition of HDPE. Bera et al. [39] prepared a series of polystyrene/silica nanocomposites with 2–30 mass% of the nanofiller content. It was found that the highest thermal stability of the nanocomposite belongs to

Table 6 Degradation parameter based on Coat-Redfern method and integral master curves of all degradation stages

Type of samples	Stage 1			Stage 2			Stage 3		
	$*E_a$	*ln A	Model	$*E_a$	*ln A	Model	$*E_a$	*ln A	Model
PBA-a	95	11.55	F1	116	13.6	F1	147	16.47	D3
10 mass% nano-SiO_2-filled PBA-a				157	19.1	D3	208	23.9	D3
20 mass% nano-SiO_2-filled PBA-a				157	18.7	D3	203	22.5	D3
30 mass% nano-SiO_2-filled PBA-a				153	18.2	D3	205	22.5	D3

the 18 mass% silica content sample. Due to nanoparticle agglomeration in the sample containing silica above the optimum loading, the thermal stability of the samples implying that is decreasing the systems turn from nano-structure to microstructure composites [39].

From Table 6, it can be observed that the degradation of neat PBA-a at first and second stages were proved to obey the F1 mechanism. In the F1 type of mechanism, the degradation is initiated from random points that act as growth center for the development of the degradation reaction. That means random nucleation with one nucleus on the individual particle [34]. While the diffusion-controlled character (D3) of the thermal degradation processes was took place in the final stage. The similar behavior was observed in $(C_{29}H_{24}N_{205})_n$ polymeric resin by Perondi et al. [40]. The authors reported that the pyrolysis kinetics of the above polymeric resin, formed by the reaction of a polymeric isocyanate and phenolic resin, are controlled by a Fn type chemical reaction at conversions lower than $\sim$0.8 whereas at conversions above 0.8, a change in the rate-limiting step, i.e., chemical reaction to diffusion, was also observed [40]. The phenomena observed were attributed to the decrease in mobility of the reacting species possibly from the enhancement crosslink density or viscosity of the polymer at high conversion [41].

For the nano-SiO_2/PBA-a composites, the mechanism was recognized to be three-dimensional diffusion (D3) reaction for all three degradation stages. The difference in the degradation mechanisms of a polymer matrix and its nanocomposites have been observed in various systems. Montero et al. [25] observed that the presence of POSS changed the thermal degradation of an epoxy resin from first order to a mechanism controlled by diffusion.

Three-dimensional diffusion mechanism (D3) associated with the diffusion process in three dimensions. When one deal with a solid or with high viscosity melts, the mass transfer processes are rate-determining for the whole process. The decomposition products must diffuse to the surface to be evaporated through the char formed or through the nanoparticles labyrinth i.e., degradation is a faster process, while it is diffusion of the volatile products to the surface which is rate-controlling process. Therefore, the diffusion mechanism is rate-controlling process at the final decomposition stage of the neat PBZ with sufficient char formation or for all stages of our highly filled nano-SiO_2/PBA-a composites.

Conclusions

An introduction of nano-SiO_2 into PBZ was found to lead to a significant change of thermal degradation mechanism and decomposition behaviors from that of the pure matrix. Thermal stability in term of degradation temperature at 5 % mass loss of PBA-a was substantially enhanced with increasing nano-SiO_2 content. The results are likely from the relatively high loading up to 30 mass% of the nano-SiO_2 used and the ability to form stable Si–O–C bond of the benzoxazine resin with the silica nanoparticles. The reduction from three to two thermal decomposition stages, with the disappearance of the lowest thermal decomposition stage of the neat PBA-a, were observed in DTG results when the nano-SiO_2 was added in the polymer. From the kinetic analysis, activation energy of the nano-SiO_2 filled PBA-a nanocomposites was observed to be higher than that of the PBA-a. The principal degradation mechanism of the PBA-a was determined to be a random nucleation type with one nucleus on the individual particle (F1 model) while that of the PBA-a nanocomposites were best described by diffusion-controlled reaction (D3 model).

Acknowledgements This research has been supported by the Ratchadaphiseksomphot Endowment Fund of Chulalongkorn University (RES560530007-AM), the Research, Development and Engineering (RD&E) Fund through National Nanotechnology Center (NANOTEC), National Science and Technology Development Agency (NSTDA), Thailand (Project P-12-00292), and from the Japan-East Asia Network of Exchange for students and Youth Program (JENESYS), 2011, Japan. Nano-SiO_2 (Reolosil® QS-20) was kindly provided by Cobra International Co., Ltd. (Thailand).

References

1. Kumar KSS, Nair CPR. Polybenzoxazines: chemistry and properties. 1st ed. England: iSmithers Rapra Publishing; 2010.
2. Ishida H, Agag T. Handbook of benzoxazine resin. 1st ed. Oxford: Elsevier; 2012.

3. Rimdusit S, Jubsilp C, Tiptipakorn S. Alloys and composites of polybenzoxazines: properties and applications. 1st ed. New York: Springer; 2013.
4. Aerospace product selector guide (2012) Henkel corporation.
5. Araldite benzoxazine thermoset resins selector guide (2009) Huntsman corporation.
6. Hemvichian K, Ishida H. Thermal decomposition processes in aromatic amine-based polybenzoxazines investigated by TGA and GC-MS. Polymer. 2002;43:4391–402.
7. Low HY, Ishida H. Mechanistic study on the thermal decomposition of polybenzoxazines: effects of aliphatic amines. J Polym Sci Part B. 1998;36:1935–46.
8. Hemvichian K, Laobuthee A, Chirachanchai S, Ishida H. Thermal decomposition processes in polybenzoxazine model dimers investigated by TGA–FTIR and GC–MS. Polym Degrad Stab. 2002;76:1–15.
9. Fam SB, Uyar T, Ishida H, Hacaloglu J. Investigation of polymerizationof benzoxazines and thermal degradation characteristics of polybenzoxazines via direct pyrolysis mass spectrometry. Polym Int. 2012;61:1532–41.
10. Yang P, Gu Y. Synthesis of a novel benzoxazine-containing benzoxazole structure and its high performance thermoset. J Appl Polym Sci. 2012;124:2415–22.
11. Kambour RP, Ligon WV, Russell RR. Enhancement of the limiting oxygen index of an aromatic polycarbonate by the incorporation of silicone blocks. J Polym Sci Polym Lett. 1978;16:327–33.
12. Liu YL, Wei WL, Hsu KY, Ho WH. Thermal stability of epoxy-silica hybrid materials by thermogravimetric analysis. Thermochim Acta. 2004;412:139–47.
13. Chrissafis K, Paraskevopoulos KM, Tsiaoussis I, Bikiaris D. Comparative study of the effect of different nanoparticles on the mechanical properties, permeability, and thermal degradation mechanism of HDPE. J Appl Polym Sci. 2009;114:1606–18.
14. Vassiliou AA, Chrissafis K, Bikiaris DN. Thermal degradation kinetics of in situ prepared PET nanocomposites with acid-treated multi-walled carbon nanotubes. J Therm Anal Calorim. 2010; 100:1063–71.
15. Chrissafis K, Paraskevopoulos KM, Pavlidou E, Bikiaris D. Thermal degradation mechanism of HDPE nanocomposites containing fumed silica nanoparticles. Thermochim Acta. 2009;485:65–71.
16. Pilawka R, Paszkiewicz S, Rosłaniec Z. Thermal degradation kinetics of PET/SWCNTs nanocomposites prepared by the in situ polymerization. J Therm Anal Calorim. 2013;. doi:10.1007/s10973-013-3239-4.
17. Nistor MT, Vasile C. Influence of the nanoparticle type on the thermal decomposition of the green starch/poly (vinyl alcohol)/montmorillonite nanocomposites. J Therm Anal Calorim. 2013; 111:1903–19.
18. Dorigato A, Pegoretti A, Frache A. Thermal stability of high density polyethylene–fumed silica nanocomposites. J Therm Anal Calorim. 2012;109:863–73.
19. Pal MK, Gautam J. Effects of inorganic nanofillers on the thermal degradation and UV-absorbance properties of polyvinyl acetate. J Therm Anal Calorim. 2013;111:689–701.
20. Feng Cheng HK, Sahoo NG, Lu X, Li L. Thermal kinetics of montmorillonite nanoclay/maleic anhydride-modified polypropylene nanocomposites. J Therm Anal Calorim. 2012;109:17–25.
21. Laachachi A, Ferriol M, Cochez M, Lopez-Cuesta JM, Ruch D. A comparison of the role of boehmite (AlOOH) and alumina (Al_2O_3) in the thermal stability and flammability of poly (methyl methacrylate). Polym Degrad Stab. 2009;94:1373–8.
22. Dueramae I, Jubsilp C, Takeichi T, Rimdusit S. High thermal and mechanical properties enhancement obtained in highly filled polybenzoxazine nanocomposites with fumed silica. Compos B. 2014;56:197–206.
23. Mahrholz T, Stangle J, Sinapius M. Quantitation of the reinforcement effect of silica nanoparticles in epoxy resins used in liquid composite moulding processes. Compos A. 2009;40:235–43.
24. Goertzen WK, Kessler MR. Dynamic mechanical analysis of fumed silica/cyanate ester nanocomposites. Compos A. 2008;39: 761–8.
25. Montero B, Ramırez C, Rico M, Barral L, Dıez J, Lopez J. Effect of an epoxy octasilsesquioxane on the thermodegradation of an epoxy/amine system. Polym Int. 2010;59:112–8.
26. Sanchez-Jimenez PE, Perez-Maqueda LA, Perejon A, Criado JM. Generalized master plots as a straightforward approach for determining the kinetic model: the case of cellulose pyrolysis. Thermochim Acta. 2013;552:54–9.
27. Ishida H. Process for preparation of benzoxazine compounds in solventless systems. US Patent 5,543,516. 1996.
28. Doyle CD. Estimating thermal stability of experimental polymers by empirical thermogravimetric analysis. Anal Chem. 1961;33:77–9.
29. Park SJ, Kim HC, Lee HI, Suh DH. Thermal stability of imidized epoxy blends initiated by N-benzypyrazinium hexafluoantimonate salt. Macromolecules. 2001;34:7573–5.
30. Periadurai T, Vijayakumar CT, Balasubramanian MJ. Thermal decomposition and flame retardant behaviour of SiO_2-phenolic nanocomposite. Anal Appl Pyrol. 2010;89:244–9.
31. Flynn JH, Wall LA. Thermal analysis of polymer by thermogravimetric analysis. J Res Natl Bur Stand. 1966;70A:487–523.
32. Vyazovkin S, Burnham AK, Criado JM, Maqueda LAP, Popescu C, Sbirrazzuoli N. ICTAC kinetics committee recommendations for performing kinetic computations on thermal analysis data. Thermochim Acta. 2011;520:1–19.
33. Khawam A, Flanagan DR. Solid-state kinetic models: basics and mathematical fundamentals. J Phys Chem B. 2006;110:17315–28.
34. Kissinger HE. Reaction kinetics in differential thermal analysis. Anal Chem. 1957;29:1702–5.
35. Ozawa T. Kinetic analysis of derivative curves in thermal analysis. J Therm Anal. 1970;2:301–24.
36. Coats AW, Redfern JP. Kinetic parameters from thermogravimetric data. Nature. 1964;201:68–9.
37. Koga N, Criado J. Kinetic analyses of solid-state reactions with a particle-size distribution. J Am Ceram Soc. 1998;81:2901–9.
38. Perez-Maqueda LA, Criado JM. The accuracy of Senum and Yang's approximations to the Arrhenius integral. J Therm Anal Cal. 2000;60:909–15.
39. Beraa O, Pilic B, Pavlicevic J, Jovicic M, Hollo B, Szecsenyi KM, Spirkova M. Preparation and thermal properties of polystyrene/silica nanocomposites. Thermochim Acta. 2011;515:1–5.
40. Perondi D, Broetto CC, Dettmer A, Wenzel BM, Godinho M. Thermal decomposition of polymeric resin $[(C_{29}H_{24}N_{205})_n]$: kinetic parameters and mechanisms. Polym Degrad Stab. 2012;97:2110–7.
41. Jankovic B. The kinetic analysis of isothermal curing reaction of an unsaturated polyester resin: estimation of the density distribution functions of the apparent activation energy. Chem Eng J. 2010;162:331–40.